PROCEEDINGS, Sixteenth Workshop on Geothermal Reservoir Engineering
Stanford University, Stanford, California, January 23-25, 1991
SGP-TR-134

NUMERICAL SIMULATION OF THE SUMIKAWA GEOTHERMAL FIELD IN THE NATURAL STATE

J.W. Pritchett*, S.K. Garg*, K. Ariki+, and Y. Kawano•

***S-CUBED, +Mitsubishi Materials Corporation, •New Energy and Industrial Technology Development Organization**

Introduction

This paper presents some results from a numerical simulation study of the natural state of the liquid-dominated high-temperature Sumikawa geothermal prospect (Pritchett *et. al.*, 1989). Sumikawa is located in the Hachimantai volcanic zone of the Sengan thermal area in northern Honshu, Japan. Exploratory studies have been in progress at Sumikawa since 1981 by Mitsubishi Materials Corporation (MMC) and Mitsubishi Gas Chemical Corporation (MGC); this comprehensive program incorporates a variety of geochemical and geophysical surveys and an extensive preliminary drilling investigation (now exceeding sixteen wells). The drilling program has revealed a complex geological structure and has made possible a very thorough pressure-transient testing program involving both single-well and long-term interference tests. These exploratory studies have been carried out jointly by MMC and NEDO (the New Energy and Industrial Technology Development Organization, an agency of the Japanese government).

Geological Setting

Sumikawa is located in mountainous terrain; Mt. Yake (just to the southwest of the Sumikawa area) and Mt Hachimantai (just to the southeast) are both active volcanoes. Figure 1 shows the location of the field in relation to regional structure; also shown are the locations of the operating geothermal fields at Kakkonda, Matsukawa and Ohnuma. The Sumikawa prospect lies approximately 2 km to the west of the Ohnuma geothermal power station (also operated by MMC). Ohnuma produces about 10 MW of electricity from a small (~ 0.6 km diameter) borefield immediately surrounding the power station.

A pronounced north-south trending gravity low has been identified to the north of the Sumikawa field, indicative of a graben structure (see Figure 1); the two active volcanoes (Mt. Yake and Mt. Hachimantai) and the Senosawa uplift zone obscure this feature farther south. Major regional tectonic features (faults, uplifts and depressions) strike north-south. Figure 1 also shows east-west lineaments along which the Quaternary volcanoes in the region (including Mt. Yake and Mt. Hachimantai) are aligned; these lineaments are believed to represent regional fracture zones. The geothermal activity in the Sumikawa/Ohnuma area is believed to originate from such an east-west fracture zone connecting Mt. Yake and Mt. Hachimantai, just to the south of the drilled area.

Figure 2 shows the local area, including both the Sumikawa and Ohnuma fields as well as the sub-region chosen for our numerical simulation study of Sumikawa. Within the study area, the ground surface averages ~ 1000 meters above sea level (ASL), but slopes sharply down from south (> 1300 m ASL near Mt. Yake) to north (< 700 m ASL near the Akagawa hot spring area). As shown, exploratory drilling is concentrated near the center of the study area; drilling to the north is sparse and shallow, and drilling to the south of well SA-2 is precluded by the Towada-Hachimantai National Park boundary. The high well density in the central part of the study area provides good resolution of the underlying geological structure. Figures 3 and 4 illustrate vertical geological sections (based on drilling logs) corresponding to sections A–A′ (east-west) and B-B′ (north-south) shown in Figure 2, respectively. Figure 3 indicates that the Sumikawa prospect lies on the western boundary of the regional north-south graben structure, with substantial downward displacements (> 1 km) in deep layers from west to east. The major geological formations in the area are as follows, in order of increasing depth:

"ST" Formation: Surficial andesitic tuffs, lavas and pyroclastics of Recent origin.

"LS" Formation: Lake sediments; Pleistocene tuffs, sandstones, siltstones and mudstones.

"DA" Formation: Pliocene dacites, dacitic tuffs and breccias.

"DI"Formation: Dacitic dike located in the extreme northwest of the study area.

"MV" Formation: "Marine/Volcanic Complex"; interbedded Miocene dacitic volcanic rocks and "black-shale" marine sediments.

"AA" Formation: Altered andesitic rocks which are apparently extensively fractured.

"GR" Formation: Crystalline intrusive rocks, mainly granodiorite and diorite.

Hydrological Characteristics

Measured underground temperatures at Sumikawa exhibit substantial dependences upon both depth and north-south position. As shown in Figure 5, temperatures at sea level elevation (~ 1 km depth) decline sharply to the north. This temperature distribution supports the hypothesis that the source of the geothermal fluids at depth is the inferred east-west deep fracture zone which connects the Mt. Yake and Mt. Hachimantai volcanoes. The highest temperature measured so far at Sumikawa is near bottomhole in well

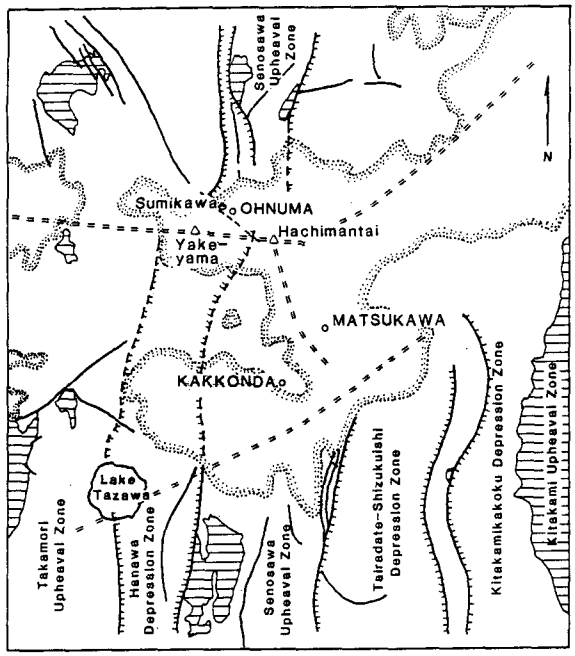

Figure 1. Area considered in mathematical simulation studies, showing computational grid spacing and well locations.

SA-2 (320°C), which is also the southernmost well at Sumikawa. Shut-in temperature surveys in the deepest wells show evidence of temperature inversions (maximum temperatures above bottomhole) which is suggestive of substantial convective heat transfer at depth.

Determinations of stable shut-in feedpoint pressures in the Sumikawa wells indicate that at relatively shallow depths (above ~ 300 m ASL), underground pressures vary horizontally and that a large shallow region of sub-hydrostatic vertical pressure gradient is present in the southern part of the area (near Mt. Yake), which is indicative of the presence of a shallow two-phase flow region in the southern part of the field. At greater depths, however, stable pressures are remarkably uniform: pressure depends only on elevation with respect to sea level, with an average gradient around 80 bars per kilometer of depth (hydrostatic for ~ 240°C).

Substantial natural outflows of hot fluids at the surface are observed at Sumikawa, mainly from a series of hot spring areas which is oriented approximately north-south and which lies midway between the Sumikawa and Ohnuma fields. Within the present study area, the major natural discharge points are the Sumikawa and Akagawa hot springs in the northeastern part of the study area. Additional hot spring areas are present farther north, which appear to be part of the same hydrological system. The total heat output from these surface discharges is of order 30 MW.

Reservoir fluids at Sumikawa may be regarded as pure H_2O for the purposes of reservoir engineering studies. Salinities are generally low (< 5000 ppm) and the incondensable gas content is typically less than one part per thousand by volume of the steam.

Many of the exploratory wells in the Sumikawa area have been discharged for periods of time ranging from a few hours to several months. Several fluid-injection tests have also been conducted. Discharge enthalpies from some of these wells are significantly in excess of saturated liquid values: in a few cases (wells S-1, SA-2 and SA-4), discharge enthalpies corresponding to pure saturated steam have been observed. This implies that these wells are producing from an underground two-phase zone within the reservoir. The most productive well at Sumikawa is also the deepest (well SN-7D, 2486 m): SN-7D is capable of discharging fluid at rates around 150 kg/s with wellhead enthalpy near 1200 J/g from feedzones located within the deepest ("GR") formation. Most other productive wells at Sumikawa withdraw fluid from the shallower "AA" formation.

A substantial body of pressure-transient data has been collected using downhole capillary-tube gauges from a number of wells in the field during these flow tests (Maki, Pritchett and Garg, 1988; Garg *et. al.*, 1991). Measurements have been performed both in flowing wells and in shut-in observation holes. Briefly, the results of the pressure transient experiments may be summarized as follows. On the whole, permeabilities at Sumikawa are both heterogeneous and highly anisotropic. Interference tests have shown that north-south communication is often quite good, whereas east-west communication is poorer and vertical communication is very low, on the average.

Apparently, the lake sediment ("LS") formation acts as a caprock for the geothermal reservoir—the absence of this formation and the relatively low ground surface elevations in the northeastern part of the study area are responsible for the substantial fluid discharges observed at the Akagawa and Sumikawa hot spring areas. Permeabilities in the "DA" formation are moderate (of the order of 10 millidarcies, depending somewhat on depth). The "marine/volcanic complex" (MV formation) is highly anisotropic, with moderate horizontal permeability but very low average vertical permeability. The "altered andesite" AA formation is quite permeable, particularly in the north-south direction—pressure test interpretations yield values in excess of 100 millidarcies. Finally, pressure-transient evidence from well SN-7D has revealed the presence of a very deep permeable horizon within the "GR" layer as well. Thus, three of the formations at Sumikawa ("DA", "AA" and "GR" appear to be fairly permeable; the "LS" layer is an impermeable aquitard, and the "MV" formation, while permeable to horizontal fluid motion, acts as a barrier to vertical flow. All rock permeability at Sumikawa is presumably due to the presence of fractures, since laboratory tests of cores indicate essentially no matrix permeability in any of these formations.

Numerical Representation

The objective of our study was to develop a mathematical representation of the Sumikawa area in the natural state. The approach was to use a numerical reservoir simulator and, starting from essentially arbitrary but physically plausible initial conditions, to compute a time-dependent evolution of the system toward an essentially steady condition. Then, computed results and observed facts were compared, and appropriate adjustments in available free parameters were made to try to improve the match between computations and observations. The entire time-dependent calculation was then repeated using these revised parameter values, and results were again compared

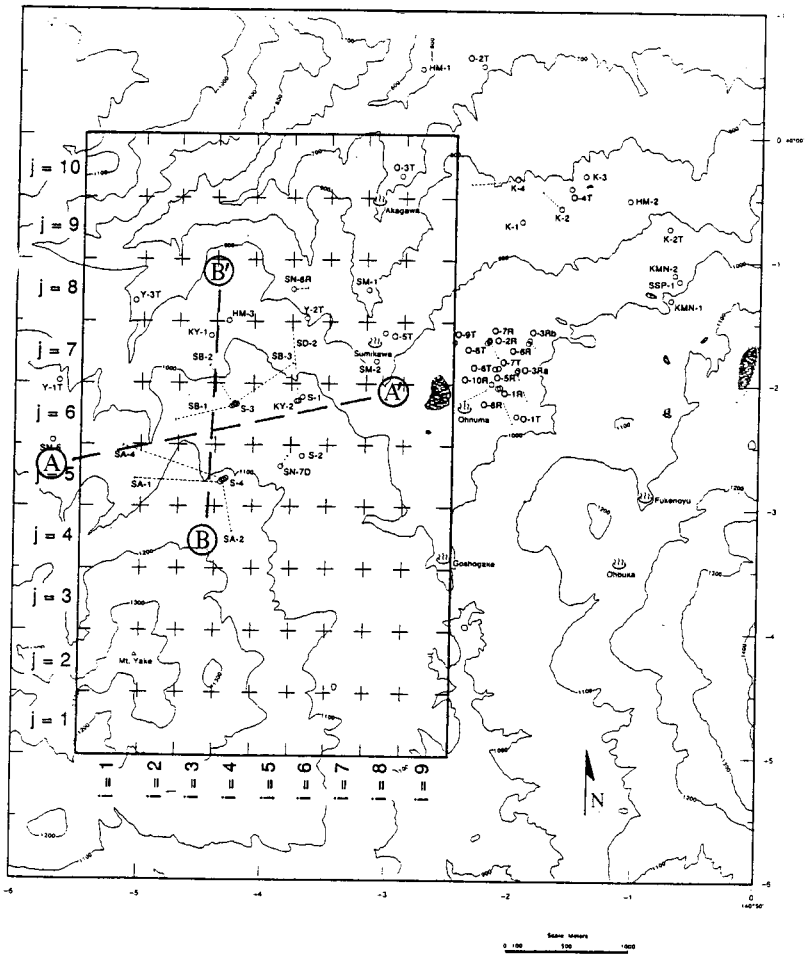

Figure 2. Tectonic map of the Sumikawa area.

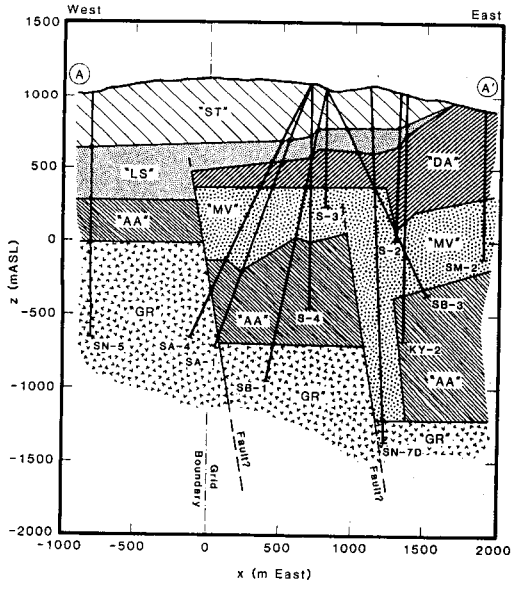

Figure 3. East-west A–A′ geological cross-section through the Sumikawa area.

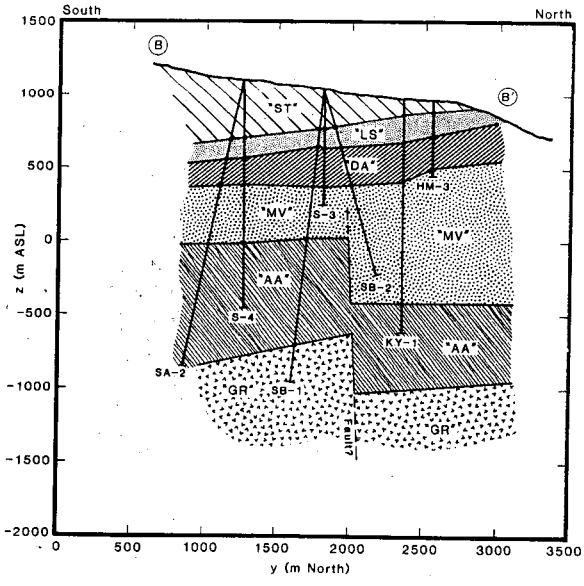

Figure 4. North-south geological cross-section B–B′ through the Sumikawa area.

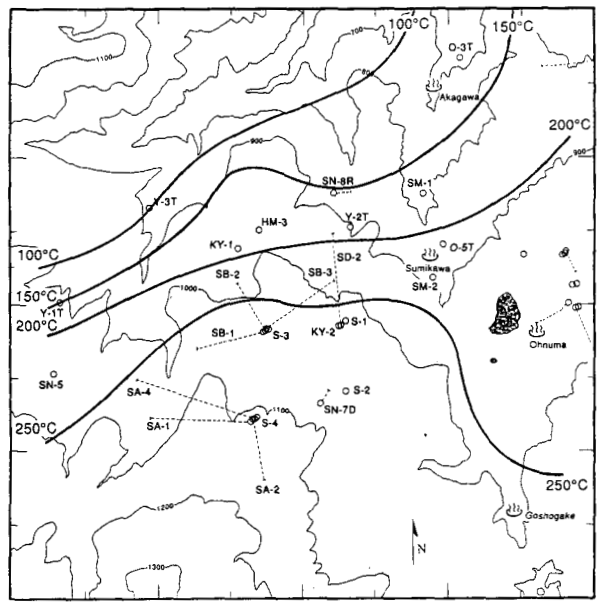

Figure 5. Temperatures at sea-level elevation in the Sumikawa/Ohnuma area.

with observations. This iterative process was repeated until a satisfactory match between computed properties (pressures, temperatures, surface discharge rates, etc.) and field observations was achieved. For this purpose, 42 such long-term calculations were required.

For this study, the STAR geothermal reservoir simulator was employed (Pritchett, 1989). All rock formations were treated as porous media, and the fluid was treated as pure H_2O. As discussed by Pritchett and Garg (1990), despite the fact that Sumikawa is a fracture-dominated reservoir, a porous-medium representation may be employed to describe the system in the natural state. A three-dimensional grid system was used, with 10 grid blocks (each 500 meters in size) in the north-south direction, 9 grid blocks (300 to 500 meters in size) in the east-west direction (see Figure 2), and a total of 16 vertical layers, ranging from 100 to 300 meters in vertical thickness. The horizontal grid area is $3 \times 5 = 15$ square kilometers, and the grid extends vertically from –1600 m ASL to +1200 m ASL; the total number of grid blocks is 1440, but some of the uppermost grid blocks are "void" owing to the irregular topography at Sumikawa.

A maximum time-step size of 8 years was employed, and most of the calculations were carried out to 30,000 years, requiring nearly 4000 time-steps per case. As initial conditions, it was simply assumed that temperature varied linearly between air temperature (10°C) at the ground surface and 250°C at –1600 m ASL (the bottom of the grid) at $t = 0$. This is substantially colder than the present temperature distribution, so that the system heated up during the time-dependent calculations. These initial conditions correspond to all-liquid conditions everywhere (no steam is present underground at $t = 0$).

Formation Properties and Boundary Conditions

Numerous free parameters were available for optimizing agreement between calculations and measurements; these were varied, as appropriate, from one calculation to the next. Basically, the free parameters included (1) certain parameters establishing the boundary conditions on the perimeter of the computing volume, (2) those rock formation permeabilities which were not constrained by pressure transient test results, and (3) the detailed geological structure where it was not well-established by drilling evidence (particularly in the southern part of the study area). In the remainder of this paper, we will present the results of the final calculation (Case 42), which appears to adequately represent the natural-state prevailing in the Sumikawa field.

Many of the required rock properties (porosity, density, heat capacity, thermal conductivity, compressibility) were treated as invariant during the study: these properties were obtained by averaging the results of laboratory tests performed upon core samples from the field. These values are listed in Table I. Furthermore, for all calculations, it was assumed that capillary effects could be neglected, and that the relative permeability functions could be treated as straight lines with residual steam saturation = 0.05 and residual liquid saturation = 0.3.

Table 1. Rock physical properties assumed for numerical simulations.

Formation	Porosity	Grain Density (kg/m^3)	Elastic Modulus (kbar)	Grain Heat Capacity (J/kg/deg)	Grain Conductivity (W/m/deg)
"ST"	0.11	2640	200	1000	1.9
"LS"	0.34	2690	200	980	2.9
"DA"	0.15	2640	300	940	3.0
"DI"	0.15	2640	300	940	3.0
"MV"	0.10	2660	500	910	3.3
"AA"	0.04	2730	600	830	2.5
"GR"	0.02	2710	600	750	3.0

Not surprisingly, the most important rock properties are the absolute permeabilities in the various coordinate directions. Some of these values were established (or at least constrained) by the results of pressure-transient tests, as discussed above; the remainder were treated as free parameters in the matching process. The final values are listed in Table II. Note that the "ST", "LS" and "DA" formations were treated as homogeneous and isotropic, with permeabilities of 1, 0.01 and 10 millidarcies respectively. The "MV" ("marine/volcanic complex") formation was treated as anisotropic, with 1 millidarcy vertical permeability and depth-dependent horizontal permeability. The extremely permeable "AA" formation was treated as very anistropic and was also subdivided into a "northern" and "southern" part, based mainly on pressure-transient evidence. Also note that all vertical permeabilities in the two deepest layers along the southern boundary of the grid were set to 10 millidarcies, irrespective of the type of rock present—this was done to represent the presumed "fracture zone" which connects Mt. Yake and Mt. Hachimantai and which provides the conduit for the hot fluids which charge the Sumikawa aquifers.

Table 2. Rock permeabilities used in final Sumikawa natural-state simulation.

Formation	Absolute Formation Permeability			Location*
	x-direction (east-west)	y-direction (north-south)	z-direction (vertical)	
"ST"	1.00 md	1.00 md	1.00 md	everywhere
"LS"	0.01 md	0.01 md	0.01 md	everywhere
"DA"	10.00 md	10.00 md	10.00 md	everywhere
"DI"	0.50 md	0.50 md	0.50 md	everywhere
"MV"	10.00 md	10.00 md	1.00 md	above 50 m ASL; $k > 6$
	2.00 md	2.00 md	1.00 md	below 50 m ASL
"AA"	20.00 md	200.00 md	2.00 md	north of -3000 m N; $j > 4$
	20.00 md	20.00 md	10.00 md	south of -3000 m N
"GR"	60.00 md	60.00 md	0.10 md	within "deep permeable zone"**
	0.10 md	0.10 md	0.10 md	elsewhere

*Note: all grid blocks with $j = 1$, $k = 1$ or 2 are assigned vertical permeability = 10.00 md to represent upflow region fracture zone along southern grid boundary at depth.

**Deep permeable zone restricted to deepest layer ($k = 1$) below −1300 m ASL; includes blocks [1,1,1], [1,2,1], [1,3,1], [2-9,1-10,1].

Each of the 1440 grid blocks was assigned one or another of the above rock formations (or was flagged "void") for purposes of each calculation. As noted above, this assignment of rock formations to individual grid blocks was constrained by drilling data in the central part of the study area, but a certain degree of latitude was permitted outside the drilled area. As an illustration, Figure 6 shows the assignments finally made to the grid blocks in the north-south section "$i = 3$". Note the resemblance between the central part of Figure 6 and Figure 4.

The fundamental character of the boundary conditions imposed on the various grid boundary surfaces did not change from case to case, but the values of many of the pertinent parameters involved were permitted to change. Provision was made for both mass and heat flow through the upper surface of the computational grid (that is, through the horizontal upper faces of the uppermost non-void grid blocks in each of the $[i,j]$ vertical columns of blocks). For pressure, the boundary condition was imposed by requiring that the mass flow through this upper surface be sufficient to maintain the pressure in each such uppermost block at its initial value, which was taken to depend only upon the distance of the center of the uppermost grid block below the local ground surface, as established by topographic maps. Optimum results were obtained by assuming that the one-bar surface (water table) lies 158 meters below the local ground surface, on the average. The temperature within each such uppermost grid block was likewise fixed at the initial value, given by assuming an air temperature of 10°C and a shallow temperature gradient of 0.1°C per meter of depth.

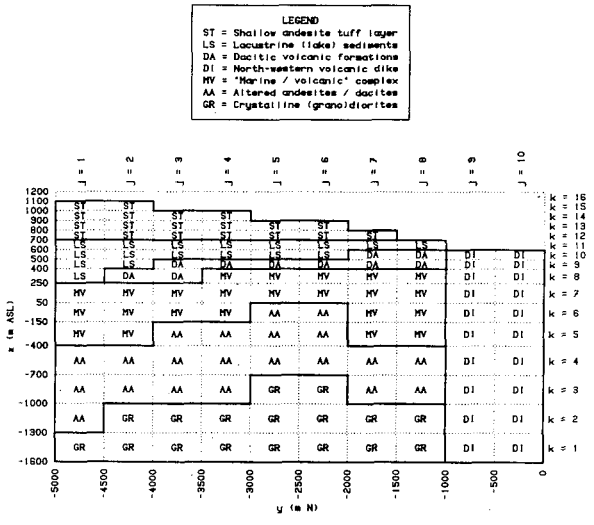

Figure 6. North-south vertical section through grid blocks with east-west index i = 3 (–4700 m E to –4400 m E). Solid lines separate grid blocks containing different rock formations; broken lines separate grid blocks within the same formation. Empty blocks above the surface are not delineated.

The bottom surface of the computational grid was treated as impermeable, but a uniform upward conductive heat flux was imposed—the final value was 0.4 watts per square meter (equivalent to 6 MW over the entire lower surface). The east and west vertical faces of the grid were treated as impermeable and insulated. Impermeable and insulated conditions were likewise imposed along most of the southern vertical surface, but in the deepest layer a mass-source of hot fluid was imposed along this boundary, representing the inflow of deep hot water from the deep Mt. Yake-Mt. Hachimantai fracture zone. As shown in Figure 7, although the mass inflow rate was uniformly distributed (and totaled 10 kg/s in the final calculation), the specific internal energy of the inflowing fluid was highest to the west (near the Mt. Yake volcano). The thermal input power represented by this deep inflow zone amounts to ~ 25 MW, significantly in excess of the 6 MW conductive heating; the total is 31 MW, in good agreement with available estimates of surface heat flow from the area. These parameter values were all adjusted several times during the course of the series of calculations. Finally, along the northern vertical face of

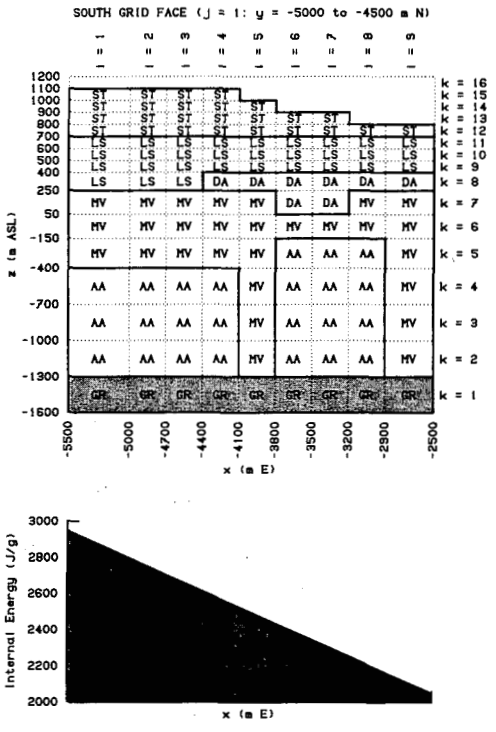

Figure 7. Upper: Southernmost vertical east-west plane of grid blocks. Shaded grid blocks contain fluid sources representing hot upflow from depth. Upflow rate is uniform, total is 10 kg/s. Lower: Internal energy of inflowing fluid varies linearly from 2950 J/g at x = –5500 m E to 2050 J/g at x = –2500 m E.

the grid, most of the surface was treated as impermeable and insulated, but a mass-sink was imposed in a single subsurface grid block located at the top of the permeable "AA" aquifer in the northeast corner of the grid (see Figure 8) to represent fluid flowing northward out of the study area which presumably supplies the hot spring areas to the north of the study area boundary. The mass withdrawal rate along the northern boundary was varied from case to case—the final value selected was 10 kg/s, which (coincidentally) is the same as the deep inflow rate from the southern boundary. Therefore, in the final model, no net inflow or outflow of fluid occurs at depth—the 10 kg/s inflow from the south is balanced by the 10 kg/s outflow to the north.

The Computed Natural State

The Case 42 calculation was carried out to t = 30,000 years, by which time essentially steady conditions prevail. Figure 9 shows how the total thermal energy within the computing volume changed with time—also shown is the derivative with time of this quantity (the net input power). Note that, at early times, an oscillation (of period ~ 1000 years) can be observed in the net input power. This oscillation is not of numerical origin, since the computational time-step is much shorter (8 years). The oscillation dies out after significant quantities of steam have formed underground. These oscillations are associated with a periodic convective pattern which develops at early times. Although these oscillations may be of interest from an academic point of view, they do not persist long so the matter was not pursued in detail.

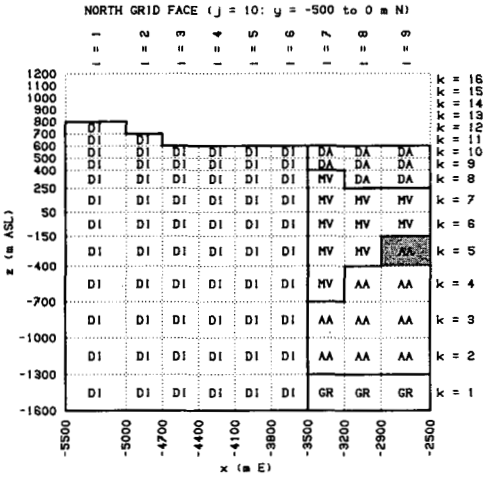

Figure 8. Northernmost vertical east-west plane of grid blocks. Shaded grid block contains fluid sink (10 kg/s) representing northern outflow from grid toward Zenikawa, Toroko and Shibari.

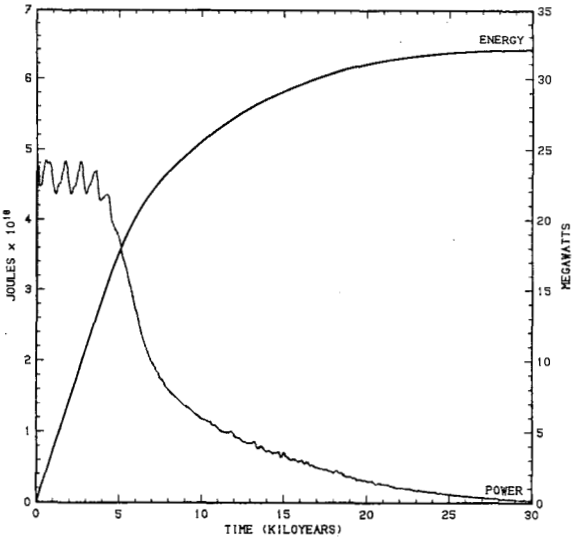

Figure 9. Change in total grid thermal energy versus time and net input power versus time for natural state calculation.

Figures 10 and 11 show north-south cross-sections for i = 3 and i = 8 (respectively). The section depicted in Figure 10 is the same as shown in Figure 6, and passes through the most extensively drilled portion of the Sumikawa field. The section in Figure 11 is farther east, and passes through the natural surface discharge areas (the Akagawa and Sumikawa hot springs). These cross-sections show (as contours) the distributions of stable subsurface temperature. Also shown (as small arrows) is the

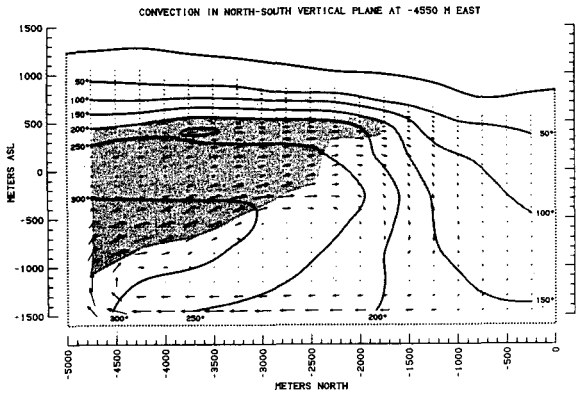

Figure 10. Computed nature-state fluid mass flux distribution in north-south vertical plane at x = –4550 m E (i = 3). Contours represent natural-state temperature. Shaded area indicates location of two-phase region.

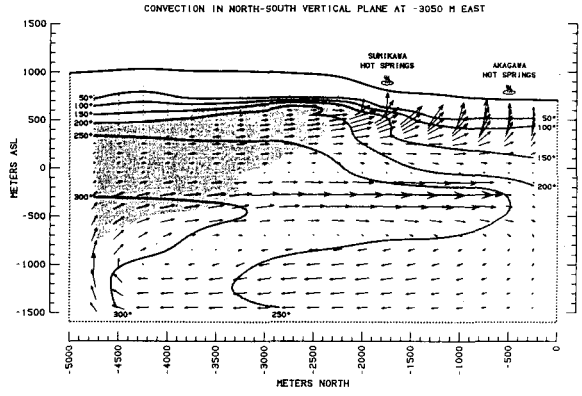

Figure 11. Computed natural-state fluid mass flux distribution in north-south vertical plane at x = –3050 m E (i = 8). Contours represent natural-state temperature. Shaded area indicates location of two-phase region.

Table 3. Comparison between computed and measured temperatures.

Well	Elevation (m ASL)	Temperature (Celsius) Computed	Measured	Difference
O-5T	+80	210.4	210	+0.4
Y-2T	+290	172.0	170	+2.0
Y-3T	+405	59.9	60	−0.1
KY-1	−570	200.9	200	+0.9
KY-2	−675	260.1	260	+0.1
S-4	−410	289.1	290	−0.9
SA-1	−690	272.6	280	−7.4
SA-2	−340	297.4	300	−2.6
SA-4	−130	269.6	270	−0.4
S-3	+350	232.2	230	+2.2
SB-1	−550	256.5	260	−3.5
SB-2	−220	238.2	240	−1.8
SB-3	+170	242.1	240	+2.1
SN-7D	−1220	241.4	240	+1.4

Table 4. Comparison between computed and measured pressures.

Well	Elevation (m ASL)	Pressure (bars) Computed	Measured	Difference
O-5T	+ 80	52.4	55	−2.6
KY-1	− 570	103.8	104	−0.2
S-2	+ 130	50.4	52	−1.6
S-4	− 410	92.1	93	−0.9
SA-1	− 690	112.3	114	−1.7
S-3	+ 350	32.5	33	−0.5
SB-1	− 550	102.3	103	−0.7
SB-2	− 220	77.3	78	−0.7
SB-3	+ 170	46.4	46	+0.4
SN-7D	−1220	151.0	149	+2.0

underground fluid mass flux distribution and (as a shaded area) the spatial extent of the two-phase (water/steam) flow zone. The unshaded area contains no underground *in-situ* steam. The relationship between the underground fluid flow pattern and the temperature distribution is reasonably clear. It is noteworthy that two distinct convection systems are apparently present—the deeper in the "AA" and "GR" deep permeable formations, and the shallower above the "MV" aquitard.

Comparisons between stable temperatures measured at the feedpoints of shut-in wells and corresponding computed temperatures (obtained by linear interpolation among principal grid point values) are indicated in Table III. Clearly, the computed temperature distribution represents the measured values about as well as could reasonably be expected: most of the computed values are within 3°C of measured temperatures. Also, the surface manifestation of the computed underground flow pattern (the calculated distribution of surface discharge) corresponds well with observations. The total computed upflow (total upflow from those surface blocks in which the flow direction is upward) for the entire surface is 37 kg/s. Four-fifths of this discharge emanates from just four grid blocks (i = 8; i = 7–10) in the northeastern part of the grid, where the hot springs at Sumikawa and Akagawa are located.

Finally, Figure 12 shows how the computed natural-state pressure distribution compares with measured stable feedpoint pressure values in wells. Agreement is seen to be quite good. Quantitative comparisons between measured and computed downhole pressures are provided in Table IV.

Accordingly, it is believed that the mathematical representation outlined above represents the Sumikawa geothermal system about as well as it can be represented

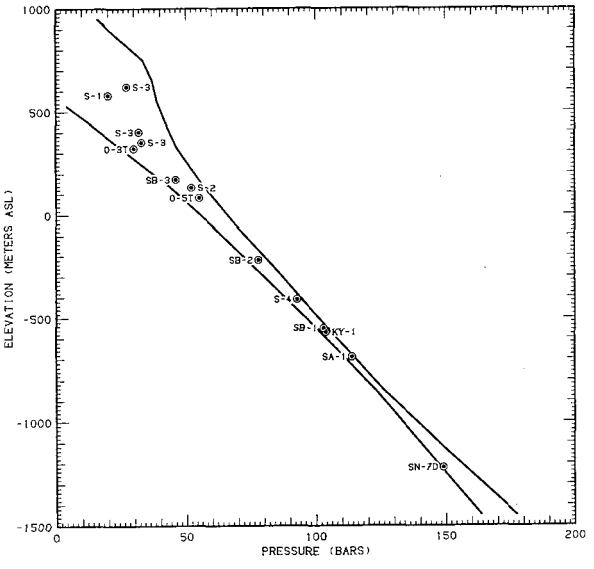

Figure 12. Comparison between measured downhole feedpoint pressures in wells and computed pressures. Solid lines indicate range of computed pressures (over grid horizontal area) for fixed elevations.

given the existing state of knowledge about the field. Parametric calculations (using the above natural-state mathematical model as a starting point) to predict system response under exploitation for electrical power have also been carried out, and indicate that the field should be capable of delivering sufficient steam for a power station of 50 MWe capacity or more for at least fifty years. Accordingly, we believe that the Sumikawa field is an excellent candidate for future development for electrical power.

References

Garg, S. K., J. W. Pritchett, K. Ariki and Y. Kawano (1991), "Pressure Interference Testing of the Sumikawa Geothermal Field", Proc. Sixteenth Workshop on Geothermal Reservoir Engineering, Stanford University.

Maki, H., J. W. Pritchett and S. K. Garg (1988), "Interpretation of a Pressure Interference Test of the Sumikawa Geothermal Field" Proc. International Symposium on Geothermal Energy 1988: Exploration and Development of Geothermal Resources, Kumamoto/Beppu, Japan.

Pritchett, J. W., S. K. Garg, H. Maki and Y. Kubota (1989), "Hydrology of the Sumikawa Geothermal Prospect, Japan" Proc. Fourteenth Workshop on Geothermal Reservoir Engineering, Stanford University.

Pritchett, J. W. (1989), "STAR User's Manual" S-CUBED Report SSS-TR-89-10242.

Pritchett, J. W. and S. K. Garg (1990), "On Similitude, Heat Conduction, and Two-Phase Flow in Fractured Porous Media", Proc. Fifteenth Workshop on Geothermal Reservoir Engineering, Stanford University.